Manipulating lipid bilayer material properties using biologically active amphipathic molecules

2006 J. Phys.: Condens. Matter 18 S1235

(http://iopscience.iop.org/0953-8984/18/28/S08)

INSTITUTE OF PHYSICS PUBLISHING JOURNAL OF PHYSICS: CONDENSED MATTER

J. Phys.: Condens. Matter **18** (2006) S1235–S1255 doi:10.1088/0953-8984/18/28/S08

Manipulating lipid bilayer material properties using biologically active amphipathic molecules

Md Ashrafuzzaman[1,3], **M A Lampson**[1,4], **D V Greathouse**[2], **R E Koeppe II**[2] **and O S Andersen**[1]

[1] Department of Physiology and Biophysics, Weill Medical College of University of Cornell, New York, NY 10021, USA
[2] Department of Chemistry and Biochemistry, University of Arkansas, Fayetteville, AR 72701, USA

E-mail: mda2001@med.cornell.edu

Received 21 February 2006, in final form 25 April 2006
Published 28 June 2006
Online at stacks.iop.org/JPhysCM/18/S1235

Abstract

Lipid bilayers are elastic bodies with properties that can be manipulated/controlled by the adsorption of amphipathic molecules. The resulting changes in bilayer elasticity have been shown to regulate integral membrane protein function. To further understand the amphiphile-induced modulation of bilayer material properties (thickness, intrinsic monolayer curvature and elastic moduli), we examined how an enantiomeric pair of viral anti-fusion peptides (AFPs)—Z–Gly–D-Phe and Z–Gly–Phe, where Z denotes a benzyloxycarbonyl group, as well as Z–Phe–Tyr and Z–D-Phe–Phe–Gly—alters the function of enantiomeric pairs of gramicidin channels of different lengths in planar bilayers. For both short and long channels, the channel lifetimes and appearance frequencies increase as linear functions of the aqueous AFP concentration, with no apparent effect on the single-channel conductance. These changes in channel function do not depend on the chirality of the channels or the AFPs. At pH 7.0, the relative changes in channel lifetimes do not vary when the channel length is varied, indicating that these compounds exert their effects primarily by causing a positive-going change in the intrinsic monolayer curvature. At pH 4.0, the AFPs are more potent than at pH 7.0 and have greater effects on the shorter channels, indicating that these compounds now change the bilayer elastic moduli. When AFPs of different anti-fusion potencies are compared, the rank order of the anti-fusion activity and the channel-modifying activity is similar, but the relative changes in anti-fusion potency are larger than the changes in channel-modifying activity. We conclude that gramicidin channels are useful as molecular force transducers to probe the influence of small amphiphiles upon lipid bilayer material properties.

[3] Author to whom any correspondence should be addressed.
[4] Present address: Laboratory of Chemistry and Cell Biology, The Rockefeller University, New York, NY 10021, USA.

1. Introduction

Biological membranes are topologically closed structures that define and separate different fluid compartments. Structurally and functionally, biological membranes are dynamic mosaic entities, composed of lipid bilayers together with imbedded bilayer-spanning proteins that move in the plane of the membrane, as originally proposed in the *fluid mosaic membrane* model [82].

The lipid bilayer component's primary function is to serve as a barrier for solute movement between different, membrane-separated fluid compartments. This barrier function depends on the bilayer hydrophobic core being a poor 'solvent' for polar solutes. The *bilayer* permeability coefficient for solute X, P_X, can be described by the solubility-diffusion mechanism [22] in which P_X is approximated as

$$P_X = \alpha_X \cdot \frac{D_X}{\delta}, \tag{1}$$

where α_X is the solute partition coefficient between the bilayer core and the aqueous phase, D_X the solute diffusion coefficient in the bilayer core (which varies little among small solutes [21]), and δ the bilayer hydrophobic thickness (∼30 Å for hydrocarbon-free bilayers [81], or [48] and 40–50 Å for hydrocarbon-containing bilayers [8]). Results for a wide variety of solutes show that P_X is proportional to α_X, as approximated by the solutes' oil/water partition coefficient [21, 65, 89], with the solute diffusion coefficient in the bilayer core being similar to that in bulk hydrocarbons (10^{-6}–10^{-5} cm^2 s^{-1} [78]).

The bilayer-spanning proteins' primary function is to catalyse the selective transfer of material and information across biological membranes. In the course of catalysing this transfer, membrane proteins undergo conformational changes: the opening/closing transitions in ion channels, e.g. Unwin and Ennis [87] and Perozo *et al* [67, 68], and the shift in substrate binding site accessibility in conformational carriers and ATP-driven pumps, e.g. Toyoshima and Mizutani [86]. To the extent that these protein conformational changes involve the protein/bilayer interface, where the protein is coupled to the bilayer through hydrophobic interactions, they will perturb the bilayer immediately adjacent to the protein [5, 10, 27, 36, 74], cf figure 1. That is, protein conformational changes involve not only rearrangements within the protein, but also interactions with the environment, particularly with the host bilayer.

The bilayer perturbation, or deformation, will in general incur an energetic cost, $\Delta G^0_{\rm def}$, that contributes to the overall free energy difference between two different protein functional states (conformations), I and II ($\Delta G^{\rm I\to II}_{\rm tot}$):

$$\Delta G^{\rm I\to II}_{\rm tot} = \Delta G^{\rm I\to II}_{\rm prot} + \Delta\Delta G^{\rm I\to II}_{\rm def}, \tag{2}$$

where $\Delta G^{\rm I\to II}_{\rm prot}$ denotes the energetic cost of the protein conformational change *per se* (including contributions from interactions with the environment, such as changes in the protein/solution interface, not considered in the protein-bilayer interactions) and $\Delta\Delta G^{\rm I\to II}_{\rm def}$, the difference in bilayer deformation energy between protein conformations I and II ($\Delta\Delta G^{\rm I\to II}_{\rm def} = \Delta G^{\rm II}_{\rm def} - \Delta G^{\rm I}_{\rm def}$). Consequently, the equilibrium distribution between the different protein conformations will be given by

$$K^{\rm I}_{\rm II} = \exp\left\{\frac{-(\Delta G^{\rm I\to II}_{\rm prot} + \Delta\Delta G^{\rm I\to II}_{\rm def})}{k_{\rm B}T}\right\} \tag{3}$$

where $K^{\rm I}_{\rm II}$ denotes the equilibrium distribution coefficient between protein states I and II, T the temperature of the bilayer environment and $k_{\rm B}$ Boltzmann's constant. If $\Delta G^0_{\rm def}$ is significant, meaning $|\Delta G^0_{\rm def}| > k_{\rm B}T$, then $\Delta\Delta G^{\rm I\to II}_{\rm def}$ may be sizable, such that the equilibrium distribution between different membrane protein conformations—and the kinetics of the conformational changes—could be modulated by the bilayer in which the proteins are imbedded [5, 10, 27, 74].

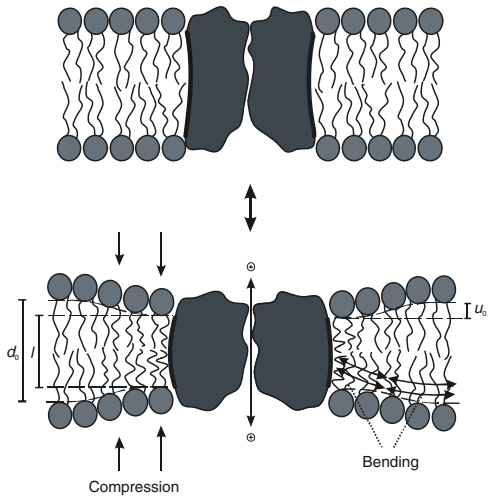

Figure 1. Hydrophobic coupling between membrane protein (ion channel) conformational changes and lipid bilayer deformations/perturbations. The hydrophobic coupling between a membrane protein and the surrounding bilayer means that a protein conformational change that involves the hydrophobic protein/bilayer boundary (indicated by the heavy black lines) will be associated with a deformation of the surrounding bilayer, which involves a local compression and bending of the two bilayer leaflets. d_0 denotes the (average) thickness of the unperturbed bilayer (d_0), l the protein's hydrophobic length and u_0 the compression of each bilayer leaflet at the protein/bilayer boundary.

(The kinetics of the conformational changes also vary as a function of the bilayer 'fluidity', but changes in fluidity cannot alter the equilibrium distribution among different conformational states; see, e.g., Lee [46].)

The success of equation (1) in predicting the passive (i.e. non-catalysed) lipid bilayer permeability coefficients for small molecules naturally leads to the notion of lipid bilayers being thin sheets of liquid hydrocarbon, stabilized by the lipid polar headgroups, as implied in the original formulation of the fluid mosaic membrane model. If that were the case, one would expect that $|\Delta G^0_{\rm def}| \ll k_{\rm B}T$, in which case membrane protein function would be little affected by changes in bilayer properties—except in cases where the interfacial surface charge densities vary [56, 60]. But lipid bilayers are not just thin sheets of liquid hydrocarbon; they are liquid crystals that exhibit both short- and long-range order [58]. By virtue of being liquid crystals, lipid bilayers also are elastic bodies [19, 31], with material properties (e.g. average thickness, intrinsic monolayer curvature and elastic moduli) that can be manipulated by the adsorption of amphipathic compounds [18, 55, 75, 79, 84, 92].

In the case of a cylindrical membrane protein of radius r_0 and hydrophobic length l, imbedded in a bilayer of average thickness d_0, intrinsic monolayer curvature c_0 and bilayer compression and bending moduli $K_{\rm a}$ and $K_{\rm c}$, the bilayer deformation can be decomposed [34] into a local bilayer compression with an associated energy density $K_{\rm a} \cdot (2u/d_0)^2$, cf Mouritsen and Bloom [59], and monolayer bending with an associated energy density $K_{\rm c} \cdot (\nabla^2 u - c_0)^2$, cf Gruner [26], where $u = (d_0 - d)/2$ with d being the local bilayer thickness (cf figure 1). Combining these contributions, one can estimate $\Delta G^0_{\rm def}$ using the theory of elastic bilayer deformations [13, 30, 34, 62, 63, 73]:

$$\Delta G^0_{\rm def} = \int_{r_0}^{\infty} \left\{ K_{\rm a}(2u/d_0)^2 + K_{\rm c}(\nabla^2 u - c_0)^2 \right\} \pi \, {\rm d}r - \int_{r_0}^{\infty} K_{\rm c}(\nabla^2 u - c_0)^2 \pi \, {\rm d}r. \qquad (4)$$

The hydrophobic match between the protein and the host bilayer means that $u(r_0) \equiv u_0 = (d_0 - l)/2$ [59] and equation (4) can be expressed as a bi-quadratic form in $d - l$ and c_0 [53, 62, 63]:

$$\Delta G^0_{\text{def}} = H_{\text{B}}(d_0 - l)^2 + H_{\text{X}}(d_0 - l)c_0 + H_{\text{C}}c_0^2 \tag{5}$$

where the coefficients H_{B}, H_{X} and H_{C} are functions of K_{a}, K_{c}, d_0 and r_0 [62, 63]. The theory of elastic bilayer deformations, as expressed in equation (4), provides quantitative insight into the bilayer thickness dependence of gramicidin (gA) channel lifetimes [34, 51]. In general, however, integral membrane proteins are not cylinders with a smooth protein/bilayer boundary [47], which may affect the local lipid packing, as well as the tilt of the acyl chain director relative to the local bilayer normal (cf Nielsen *et al* [62]), and the elastic moduli adjacent to the protein may differ from the bulk values [66]. Yet, the structure of equation (5) should remain correct to the first significant order.

K_{a}, K_{c} and c_0 vary when amphiphiles adsorb at the bilayer/solution interface [18, 55, 75, 79, 84, 92]. These amphiphile-induced changes in bilayer elasticity and monolayer intrinsic curvature will modulate the ΔG^0_{def} associated with a bilayer perturbation, e.g. the deformation caused by a hydrophobic mismatch between a bilayer-spanning protein and the host bilayer. Amphiphiles that alter membrane protein function thus may alter the function by binding to the protein *per se*, thereby altering ΔG^0_{prot} [11, 37, 40], and by adsorbing to the bilayer, thereby altering ΔG^0_{def} [4, 52, 53].

Even in cases where amphiphiles adsorb (only) at the bilayer/solution interface, could any changes in bilayer elasticity be due to more specific amphiphile–lipid or amphiphile–protein interactions at the protein/bilayer boundary? To address this question, and to evaluate tools that could be used in more complex systems, we examined whether anti-fusion peptides (AFPs) that originally were used to inhibit the fusion of paramyxoviruses and myxoviruses with mammalian cells [71, 72] alter bilayer elasticity. Richardson and Choppin showed that a diverse group of small peptides, such as Z–D-Phe–L-Phe–Gly, where Z denotes a benzyloxycarbonyl group, inhibit viral fusion. Enantiomeric pairs of such AFPs were equally effective, which suggests a physical rather than a specific chemical basis for the AFP action. Indeed, Z–D-Phe–L-Phe–Gly inhibits the fusion of phospholipid vesicles [42] and destabilizes phospholipid structures with small negative radii of curvature [90], as would be expected for molecules that inhibit the formation of non-bilayer fusion intermediates [70]. Unexpectedly, however, Z–D-Phe–L-Phe–Gly had little effect on phospholipid structures with large radii of curvature [90], which raises the question of whether the adsorption of AFPs to lipid bilayers could alter bilayer properties other than the intrinsic curvature.

We focus primarily on the simple AFP Z–Gly–Phe and its enantiomer Z–Gly–D-Phe, and examine how they alter bilayer properties using gA channels as probes of changes in bilayer properties [4, 52]. Specifically, we wish to determine whether any AFP-dependent changes in bilayer properties could result from 'simple' changes in global bilayer properties (changes in elastic moduli or intrinsic curvature). In that case, one would expect peptides of different chirality to have similar effects on gA channel function. Otherwise, one would need to consider also local, and more specific, AFP–gA channel interactions. In order to provide further insight into this question, and to investigate whether there is a correlation between the anti-fusion activity of AFPs and any effect on bilayer physical properties, we also did experiments with Z–D-Phe–L-Phe–Gly and Z–Phe–Tyr.

The principles underlying the use of gA channels as probes of bilayer properties are illustrated in figure 2.

The atomic resolution structure of gA channels is well established, with the channels being dimers of two right-handed, $\beta^{6.3}$-helical subunits [6, 43, 85]. The bilayer-spanning channels

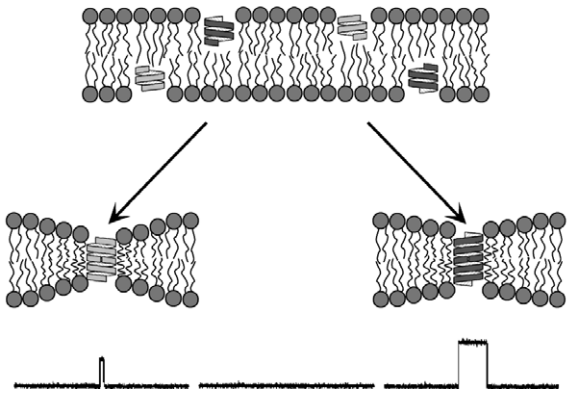

Figure 2. Gramicidin channel formation and lipid bilayer deformations. Non-conducting $\beta^{6.3}$-helical gramicidin subunits, are imbedded in each bilayer leaflet [29]. As the subunits diffuse in the plane of each leaflet, they will encounter subunits in the opposite leaflets. A small fraction of these encounters lead to the formation of bilayer-spanning channels [7, 9], which causes a bilayer deformation that involves the compression and bending of the bilayer leaflets adjacent to the channel. In the present experiments we used two different gA analogues that differed in length and helix sense. The symmetric, homodimeric channels formed by the different analogues can be distinguished by the different amplitudes of the current steps and by their different lifetimes, as indicated in the current traces at the bottom of the figure. The channels formed by analogues with the shorter, 13-residue sequences have average lifetimes that are one-tenth those of the analogues formed by the longer, 15-residue sequences—in qualitative agreement what would be expected from the larger channel–bilayer compression imposed by the shorter channels—and current transition amplitudes ∼2/3 those of the 15-residue channels.

are formed by the reversible, transbilayer association of these $\beta^{6.3}$-helical monomers [64]:

$$M_{left} + M_{right} \underset{k-1}{\overset{k_1}{\rightleftarrows}} D,$$

where M and D denote gA monomers and dimers and the subscripts denote monomers residing in each bilayer leaflet. Within limits, the channel structure is invariant when the lipid bilayer thickness is varied [41, 88], meaning that the gA channels are more rigid than the host bilayer. Consequently, when the bilayer's hydrophobic thickness is larger than the channel's hydrophobic length, as is the case in the present study, the bilayer will adjust locally to match the channel length, which incurs an energetic cost (equations (4) and (5)).[5] When a channel disappears, a transition state is reached when two of the six H-bonds that stabilize the bilayer-spanning dimer are broken [16, 57], in which case the two subunits have moved a distance δ (≈1.6 Å) apart along the channel axis. (The movement of the two subunits relative to each other is complex, involving both a rotation and a lateral axial displacement [57].)

Changes in ΔG^0_{def} will shift the equilibrium distribution between non-conducting gA monomers and conducting channels. The dimerization constant for channel formation, K, is given by

$$K = \frac{[D]}{[M]^2} = \exp\left\{\frac{-(\Delta G^0_{prot} + \Delta G^0_{def})}{k_B T}\right\} \tag{6}$$

where ΔG^0_{prot} denotes the energetic contributions due to the channel subunit–subunit

[5] The local lipid packing will be perturbed whenever $d_0 \neq l$, but the analysis becomes particularly simple when $d_0 > l$, in which case the perturbation can be approximated as a local bilayer thinning because the channel axis should be coincident with the bilayer normal, as shown in solid-state NMR experiments [12, 44, 61].

interactions. Because $\Delta G^0_{\rm def}$ varies as a function of $d_0 - l$, the bilayer will respond to the deformation by imposing a disjoining force, $F_{\rm dis}$, on the bilayer-spanning channels:

$$F_{\rm dis} = -2H_{\rm B}(d_0 - l) - H_{\rm X} \cdot c_0. \tag{7}$$

Changes in $F_{\rm dis}$ will be observable as changes in channel lifetime, τ, which means that gA channels become molecular force transducers imbedded in the lipid bilayers [4]. This is so because $\tau = 1/k_{-1}$, where k_{-1} is the dimer dissociation rate constant. The disjoining force alters k_{-1} by altering the activation energy for channel dissociation:

$$k_{-1} = \frac{1}{\tau_0} \exp\left\{\frac{\Delta G^{\ddagger}}{k_{\rm B}T}\right\} = \frac{1}{\tau_0} \exp\left\{\frac{\Delta G^{\ddagger}_{\rm prot} + \Delta\Delta G^{\ddagger}_{\rm def}}{k_{\rm B}T}\right\}, \tag{8}$$

where $1/\tau_0$ denotes the frequency factor for the reaction and $\Delta\Delta G^{\ddagger}_{\rm def}$ denotes the difference in bilayer deformation energy as the two subunits move apart to reach the transition state for dimer dissociation.

$$\Delta\Delta G^{\ddagger}_{\rm def} \approx -F_{\rm dis}\delta. \tag{9}$$

(The exact expression for $\Delta\Delta G^{\ddagger}_{\rm def}$ (cf equation (5)) is $\Delta\Delta G^{\ddagger}_{\rm def} = (2H_{\rm B}(d_0 - l - \delta) + H_{\rm X}c_0)\delta$, which reduces to equation (9) when $\delta \ll (d_0 - l)$.)

According to equations (7)–(9), if τ_0 is invariant then $\ln\{\tau\}$ should vary as a linear function of $d_0 - l$, which is the case [51]. Changes in $F_{\rm dis}$ could arise from changes in bilayer thickness, from changes in the bilayer elastic moduli (which will alter $H_{\rm B}$ and $H_{\rm X}$), and from changes in c_0. It is possible, within limits, to distinguish among these contributions in experiments using gA channels of different lengths. This is possible because $F_{\rm dis}$ can be separated into a term that reflects the hydrophobic mismatch, $-2H_{\rm B}(d_0 - l)$, and a term that reflects the intrinsic curvature, $-H_{\rm X}c_0$. If the AFPs do not alter the unperturbed bilayer thickness, any changes in the $-2H_{\rm B}(d_0 - l)$ term will result from changes in $H_{\rm B}$, i.e. from changes in the bilayer elastic moduli. For a given change in $H_{\rm B}$, $-2H_{\rm B}(d_0 - l)$ varies as a function of channel length (or, more precisely, as a function of the bilayer–channel hydrophobic mismatch). Thus, when comparing how an experimental manoeuvre (such as addition of AFPs) alters the lifetime of a longer channel, of length $l_{\rm l}$, and of a shorter channel, of length $l_{\rm s}$, a given change in $H_{\rm B}$ will cause a larger change in $-2H_{\rm B}(d_0 - l_{\rm s})$ than in $-2H_{\rm B}(d_0 - l_{\rm l})$—and a larger (relative) change in the lifetime of the shorter channel. In contrast, changes in the $-H_{\rm X}c_0$ term will be invariant with respect to changes in channel length, and cause similar (relative) changes in the lifetimes of long and short channels.

2. Materials and methods

2.1. Materials

Dioleoylphosphatidylcholine (DOPC) and diphytanoylphosphatidylcholine (DPhPC) were purchased from Avanti Polar Lipids (Alabaster, AL, USA) and used without further purification. N-decane was 99.9% pure from ChemSampCo (Trenton, NJ, USA). [Val^1]gA and its enantiomer [Val^1]gA$^-$ (with 15 amino acids in the sequences), and the gA analogue [Ala^1]gA and its enantiomer [D-Ala^1]gA$^-$ (with 15 amino acids in the sequence), as well as the sequence-shortened enantiomeric pair of analogues, des-(Val^1-Gly^2)-gA and des-(D-Val^1–Gly^2)–gA$^-$ (with 13 amino acids in the sequence), were synthesized and purified as described previously [25]. The amino acid sequences, channel lengths, phospholipids, bilayer thicknesses and abbreviations used in this article are shown in table 1.

The peptides Z–Gly–D-Phe (ZGdF), Z–Gly–Phe (ZGF), Z–D-Phe–Phe–Gly (ZdFFG) and Z–Phe–Tyr (ZFY) were purchased from Bachem (King of Prussia, PA, USA). Their structures

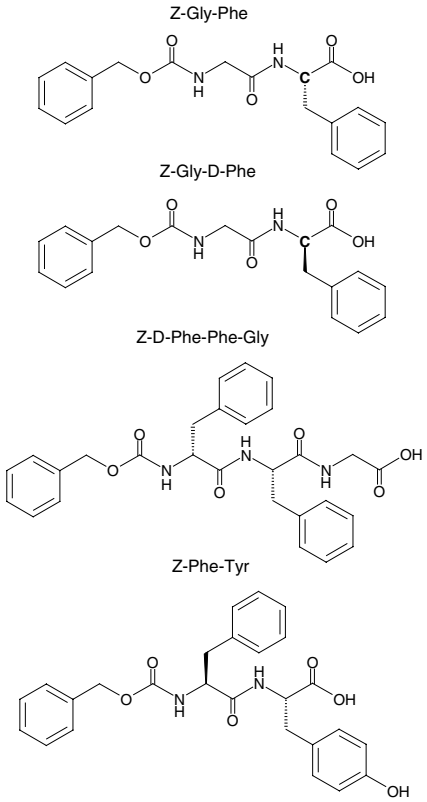

Figure 3. Structures of the peptides used in this study. The chiral centres in Z–Gly–Phe and Z–Gly–D-Phe are emphasized.

Table 1. (A) Gramicidin sequences and channel lengths. (The underlined residues are D-amino acids; f is formyl; ea is ethanolamide.) (B) Phospholipids and bilayer thicknesses.

(A)

Gramicidin analogue	Abbr.	Sequence	Hydrophobic length[a] (Å)
[Val^1]gA	VgA(15)	f-V-G-A-L-A-V-V-V-W-L-W-L-W-L-W-ea	22
[D-Val^1]gA$^-$	VgA$^-$(15)	f-V-G-A-L-A-V-V-V-W-L-W-L-W-L-W-ea	22
[Ala^1]gA	AgA(15)	f-A-G-A-L-A-V-V-V-W-L-W-L-W-L-W-ea	22
[D-Ala^1]gA$^-$	AgA$^-$(15)	f-A-G-A-L-A-V-V-V-W-L-W-L-W-L-W-ea	22
des-(Val^1–Gly^2)gA	gA(13)	f-A-L-A-V-V-V-W-L-W-L-W-L-W-ea	19
des-(D-Val^1-Gly^2)gA$^-$	gA$^-$(13)	f-A-L-A-V-V-V-W-L-W-L-W-L-W-ea	19

(B)

Phospholipid	Abbr.	Bilayer thickness[a] (Å)
Dioleoylphosphatidylcholine	DOPC	48–50
Diphytanoylphosphatidylcholine	DPhPC	42

[a] From [35].

are shown in figure 3. (The abbreviated names for the different peptides use the single-letter amino acid code, and D-residues are indicated by the prefix ‘d’.)

The electrolyte solutions were either unbuffered, or buffered with HEPES (pH 7.0) or glycine–glycine (pH 4.0), both from Sigma (St Louis, MO, USA).

2.2. Methods

Planar lipid bilayers were formed from DOPC/n-decane or DPhPC/n-decane (2.5% w/v) solutions across a 1.5 mm hole in Teflon® separating the two electrolyte solutions, using the pipette method of Szabo *et al* [83]. All experiments were done at 25 ± 1 °C, and the aqueous electrolyte solutions were 1 M NaCl, buffered to pH 7.0 using 5 mM HEPES or buffered to pH 4.0 using 10 mM glycine–glycine; 1 mM EDTA was added to the latter solutions. Some early experiments were done in unbuffered 1 M NaCl solutions. When forming the bilayers, care was taken to minimize the total amount of lipid (and *n*-decane) that was added; the total volume of the lipid/decane solution usually was 1000-fold less than the volume of the aqueous solution.

Most experiments were done in DOPC/n-decane bilayers with a 15-residue and a 13-residue gA analogue of opposite chirality, e.g. AgA(15) and $gA^-(13)$, an experimental design that allows for a direct test of how changes in hydrophobic mismatch may affect the anti-fusion peptides' action (figure 2). The reason for using gA analogues of opposite chirality is that this experimental design ensures against the formation of heterodimers between the 13-amino acid and 15-amino acid analogues [45], which would complicate the data analysis. Some early experiments were done in DOPC/n-decane bilayers, in either unbuffered or buffered solutions, using either VgA(15) and $VgA^-(15)$, which are indistinguishable in their electrophysiological properties [45, 69]. In all experiments, the applied potential across the membrane was 200 mV.

The anti-fusion peptides were added to both aqueous solutions (both sides of the bilayer) during stirring as small aliquots of 10 or 100 mM stock solution in dimethylsulfoxide (stored at −40 °C). After peptide addition, the aqueous phases were stirred for about 5 min before the measurements resumed. The total amount of added dimethylsulfoxide was less than 0.8% of the volume of the electrolyte solution, a concentration that has no effect on gA channel function.

Single-channel experiments were done using the bilayer-punch method [3] and a Dagan 3900A patch-clamp amplifier (Dagan Corp., Minneapolis, MN) with a 3910 bilayer-expander module. The current signal was filtered at 2 kHz, digitized at 20 kHz, and digitally filtered at 200–500 Hz before the single-channel transitions were detected using the algorithm described by Andersen [3] and implemented in Visual Basic (Microsoft Corp., Redmond, WA). Single-channel lifetimes were determined as described in [77] and [15], a procedure that allows for separate determination of the lifetimes of different channel types.

The specific membrane capacitance (C_m) was measured using a sawtooth potential across planar bilayers with an area of ∼1.5 mm^2. The bilayer area was measured optically using a microscope with a calibrated reticule.

2.3. Data analysis

The average channel lifetime (τ) was estimated by fitting a single-exponential distribution

$$N(t)/N(0) = \exp\{-t/\tau\}, \tag{10}$$

where $N(t)$ is the number of channels with lifetimes longer than time t, to the lifetime distributions using Origin 6.1 (OriginLab Corp., Northampton, MA, USA).

The relative changes in channel appearance rates (f) were estimated as the ratio of channel appearance rates (for each channel type), determined using two 5–10 min recordings obtained about 10 min after the addition of the anti-fusion peptide, and two 10–20 min recordings

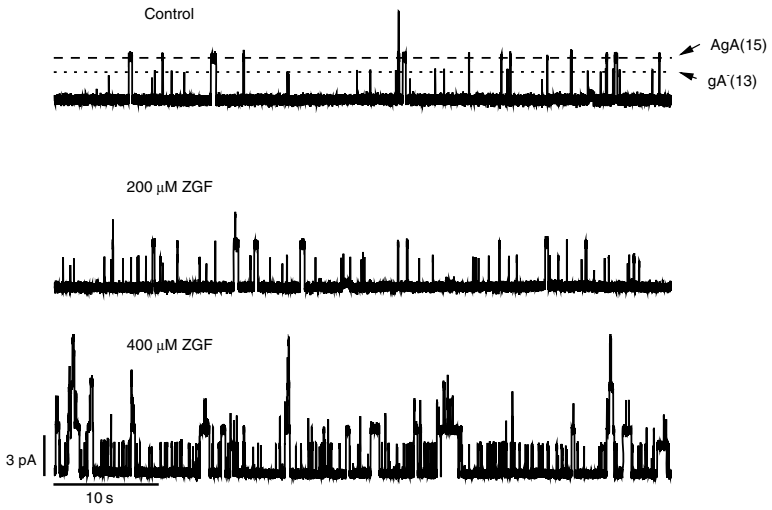

Figure 4. ZGF increases gramicidin channel activity. 60 s current traces recorded in the absence and presence of 200 or 400 μM ZGF. Two different gramicidins, AgA(15) and gA$^-$(13), were present on both sides of the bilayer. The gA$^-$(13) and AgA(15) channels can be distinguished by virtue of their different current transition amplitudes, as indicated by the two horizontal lines in the top trace: AgA(15) (- - - -) and gA$^-$(13) (· · · · · ·). DOPC, 1.0 M NaCl, pH 7.0, 25 °C, 200 mV, 500 Hz.

obtained just before the addition of the anti-fusion peptide. (The relative changes in channel appearance rate can be determined only in experiments where the bilayer does not break during the addition of the anti-fusion peptides.)

Relative changes in the time-averaged channel 'concentrations' were estimated as the product of the channel appearance rate and lifetime—measured before and after the addition of the anti-fusion peptide, i.e. as $f_{\mathrm{AFP}}\tau_{\mathrm{AFP}}/f_{\mathrm{cntl}}\tau_{\mathrm{cntl}}$, where the subscripts 'AFP' and 'cntl' denote the appearance rates and lifetimes in the presence and absence of the AFP. Again, only bilayers that did not break during anti-fusion peptide addition were used for the analysis. The amphiphile-induced changes in the free energy of dimerization $\Delta\Delta G^0_{\mathrm{tot}}$ then were determined as

$$\Delta\Delta G^0_{\mathrm{tot}} = -k_{\mathrm{B}}T \ln\left\{\frac{f_{\mathrm{AFP}}\tau_{\mathrm{AFP}}}{f_{\mathrm{cntl}}\tau_{\mathrm{cntl}}}\right\}. \tag{11}$$

Because the average lifetimes of channels formed by the three pairs of enantiomeric gA analogues vary 50-fold under control conditions, all results are reported as mean ± standard deviation of the relative changes in lifetimes, appearance rates or concentrations based on three or more independent experiments.

3. Results

3.1. Anti-fusion peptides increase gramicidin channel stability

The anti-fusion peptides are potent modifiers of gA channel function. Figure 4 shows single-channel current traces obtained before and after the addition of 200 and 400 μM ZGF to the aqueous phases bathing a bilayer in the presence of gA$^-$(13) and AgA(15). Comparable results were observed with the other combinations: gA$^-$(13) and AgA(15) in the presence of ZGdF; gA(13) and AgA$^-$(15) in the presence of either ZGF or ZGdF.

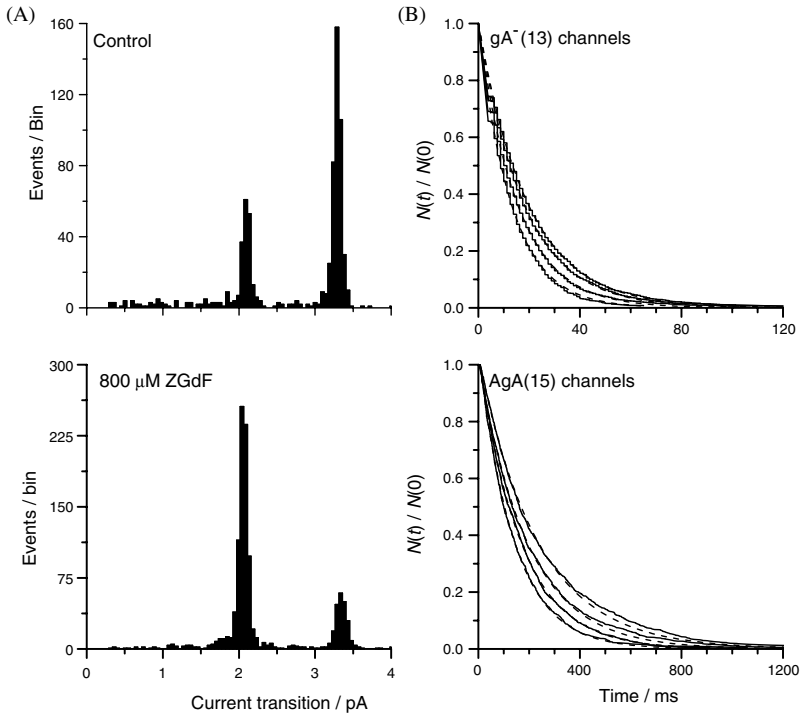

Figure 5. ZGdF has little effect on gramicidin channel current transition amplitudes (left) and increases channel lifetime (right). Left: in the current transition histograms there are two peaks, one around 2.1 pA, corresponding to the $gA^-(13)$ channels, and one around 3.3 pA, corresponding to the AgA(15) channels. In the absence of ZGdF there are 722 transitions: 188 transitions in the $gA^-(13)$ peak at 2.10 ± 0.06 pA, and 431 transitions in the AgA(15) peak 3.30 ± 0.05 pA. In the presence of 800 μM ZGdF, there are 1170 transition: 803 transitions in the $gA^-(13)$ peak at 2.06 ± 0.06 pA, and 230 transitions in the AgA(15) peak 3.34 ± 0.07 pA. Right: the lifetime distributions, plotted as survivor plots, for $gA^-(13)$ channels (top) and AgA(15) channels (bottom). The shorter $gA^-(13)$ channels have lifetimes that are one-tenth of those of the longer AgA(15) channels. Each histogram is fitted by single exponential distributions. Dashed lines denote fits of single exponential distribution to the results. Both sets of lifetime distributions show results for (from left to right) 0, 200, 400 and 800 μM ZGdF. DOPC, pH 7.0.

Two different channel types are observed: low-conductance, short-lived channels, which are $gA^-(13)$ homodimeric channels; and high-conductance, long-lived channels, which are AgA(15) homodimeric channels. (The channel types were identified in experiments where only one gA analogue was added to both sides of a bilayer.) Because the channel-forming subunits have opposite helix sense, we avoid the formation of heterodimeric channels, which would complicate the analysis [15, 45]. When the ZGF is added to the aqueous phases, there is a pronounced, concentration-dependent increase in the channel appearance rates with more modest changes in the single-channel lifetimes, and little change in the single-channel current transition amplitudes. In some experiments there was reduced bilayer stability after the addition of the AFP, but we did not observe new discrete, channel-like events due to the AFP itself; cf Sawyer and Andersen [76].

The $gA^-(13)$ and AgA(15) channels are distinguishable by virtue of the magnitude of their single-channel current transition amplitudes (figure 5, left column).

AFPs have a free carboxyl group, which is expected to have a typical pK $\approx$ 3.5 [17]. Adsorption of the AFPs at the bilayer/solution interface therefore would be expected to impart a

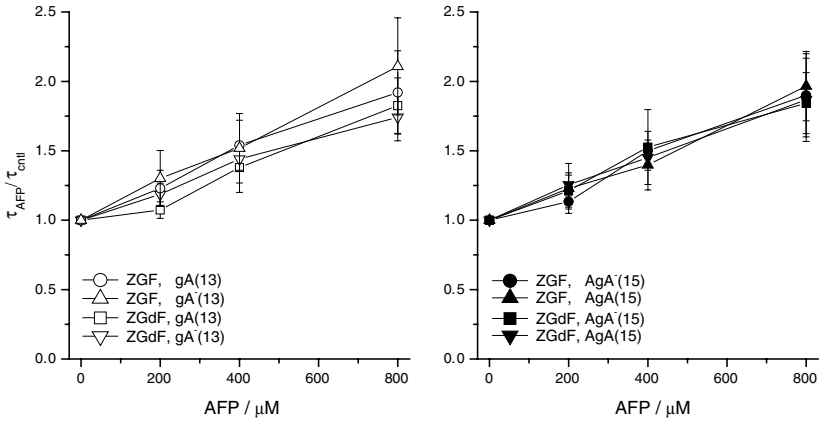

Figure 6. Effect of ZGF and ZGdF on the lifetimes of channels formed by 13-residue and 15-residue gramicidin analogues. To facilitate comparison of the results for the 13-residue and 15-residue channels, the results are displayed as τ_{AFP}/τ_{cntl} (mean $\pm$ S.D., $n \geqslant 3$). In the control experiments, the lifetimes for the gA(13) and gA$^-$(13) channels were 12.6 ± 0.3 and 14.5 ± 1.6 ms, respectively; the lifetimes for the AgA(15) and AgA$^-$(15) channels were 166 ± 20 and 152 ± 22 ms respectively. In this and the following figures, the open symbols denote results for the 13-residue channels; the closed symbols denote results for the 15-residue channels. The different symbol shapes denote the four different combinations of gramicidin analogues and AFPs: gA(13) +AgA$^-$(15) and ZGF; gA$^-$(13) + AgA(15) and ZGF; gA(13) +AgA$^-$(15) and ZGdF; gA$^-$(13) + AgA(15) and ZGdF. DOPC, pH 7.0.

negative surface charge, which would increase the interfacial [Na^+] and thus the single-channel conductance. Yet addition of the AFPs does not alter the current transition amplitude. In the absence of ZGF, the single-channel current transition amplitudes of gA$^-$(13) and AgA(15) channels are 2.14 ± 0.08 and 3.37 ± 0.13 pA, respectively ($n = 5$; 200 mV). In the presence of 800 μM ZGF, the single-channel current transition amplitudes of gA$^-$(13) and AgA(15) channels are 2.12 ± 0.05 and 3.39 ± 0.05 pA, respectively ($n = 5$; 200 mV). When the AFPs adsorb to the bilayer/solution interface, they do not appear to impart a significant surface charge—because the surface density of the AFPs is too low to build up a significant surface charge, or because the pK for adsorbed AFPs is much higher than the bulk pK.

In contrast to the invariant current transition amplitudes, the single-channel lifetime distributions vary as a function of the AFP concentration (figure 5, right column). The lifetime distributions are well fitted by single-exponential distributions (equation (10)). As expected, the shorter gA$^-$(13) channels have shorter lifetimes than the longer AgA(15) channels, reflecting the stronger F_{dis} imposed on the shorter channels (equations (7)–(9)). Somewhat unexpectedly, the relative lifetime changes are comparable for the two channel types—a result that differs from what we have observed previously with other bilayer-modifying amphiphiles [35, 50, 52].

Figures 6 and 7 summarize our results on the AFP concentration dependence of the changes in single-channel lifetimes and appearance rates for the four combinations of channel and AFP chiralities examined.

For channels formed by both the 13- and the 15-residue analogues, the relative lifetime changes (figure 6) increase as a linear function of [AFP]. This pattern is similar to that observed with other amphiphiles [35, 52, 53]. There is little difference among the eight combinations tested: gA$^-$(13) channels in the presence of either ZGF or ZGdF; gA(13) channels in the presence of either ZGF or ZGdF; AgA$^-$(15) channels in the presence of

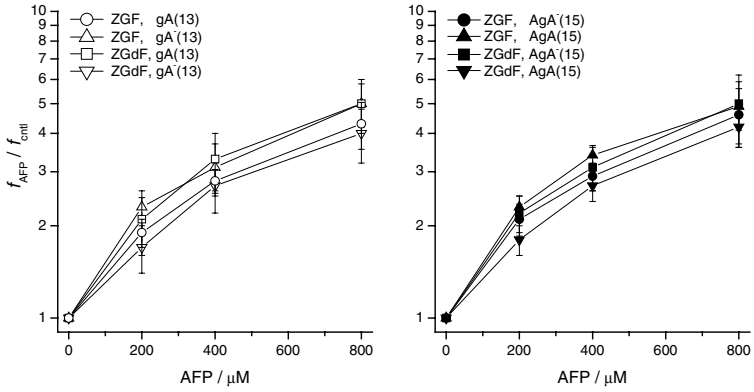

Figure 7. Effect of ZGF and ZGdF on the appearance rates of 13-residue and 15-residue gramicidin channels. The symbols have the same significance as in figure 6. DOPC, pH 7.0.

either ZGF or ZGdF; and AgA(15) channels in the presence of either ZGF or ZGdF. These results thus indicate that the AFP-induced changes in gA channel function do not result from specific AFP–channel interactions but rather from general, physical changes in bilayer material properties.

Within the framework provided by the theory of elastic bilayer deformations, the very similar changes in τ_{AFP}/τ_{cntl} show that the lifetime changes are not due to changes in bilayer elastic moduli, as expressed in the phenomenological spring constant H_B, cf equations (7)–(9). To determine whether the AFPs change lipid bilayer thickness, we measured the specific capacitance of DOPC/n-decane lipid bilayers in the absence and presence of 800 μM ZGF. In the absence of ZGF, the specific capacitance was 3.72 ± 0.24 nF cm^{-2} (mean $\pm$ S.D., $n = 11$); in the presence of 800 μM ZGF, the specific capacitance was 3.94 ± 0.38 nF cm^{-2} (mean $\pm$ S.D., $n = 10$). As is the case for other bilayer-active amphiphiles [35, 52], ZGF has no significant effect on membrane capacitance (lipid bilayer thickness) at the concentrations used here. That is, the gA channel lifetime changes seem to result primarily from changes in lipid intrinsic curvature.

For channels formed by both the 13- and the 15-residue analogues, the channel appearance rates (figure 7) increase as a linear function of [AFP] with little variation among the different combinations of channels and AFPs. Considering the scatter in the results, there is no systematic variation with respect to the identity of the channels or the AFPs; we conclude that the scatter is due to experimental fluctuations in this measurement, which inherently is relatively imprecise. The relative increases in f_{AFP}/f_{cntl} are larger than the increases in τ_{AFP}/τ_{cntl}, as expected because the local bilayer compression, $d_0 - l$, is much larger than the distance the two subunits move apart to reach the transition state for channel dissociation; see, e.g., Lundbæk *et al* [52]. Because the local bilayer compression will be larger for the shorter channel, one would expect the changes in f_{AFP}/f_{cntl} to be larger for the shorter channels. Surprisingly, this is not the case.

From the results in figures 6 and 7, one can calculate how the time-averaged channel concentrations, $f_{AFP}\tau_{AFP}/f_{cntl}\tau_{cntl}$, vary as a function of [AFP] and thus the changes in ΔG^0_{tot}; cf equation (11). The results are shown in figure 8.

The AFPs cause significant changes in the free energy of gA dimerization. The changes do not depend on chemical identify of the channels or the AFPs, which suggests that the changes in ΔG^0_{tot} result from changes in ΔG^0_{def}—and not from changes in ΔG^0_{prot}.

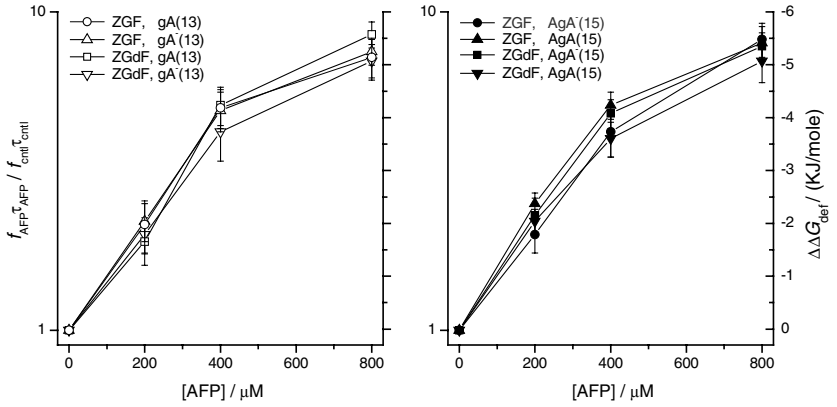

Figure 8. ZGF- and ZGdF-induced changes in the time-averaged concentrations and free energy of formation of 13-residue (left panel) and 15-residue (right panel) gramicidin channels. In each panel the left-hand ordinates denote the relative channel concentrations, expressed as $f_{\mathrm{AFP}}\tau_{\mathrm{AFP}}/f_{\mathrm{cntl}}\tau_{\mathrm{cntl}}$, and the right-hand ordinates denote the changes in the free energy of gramicidin channel formation (cf equation (11)). The symbols have the same significance as in figure 6. DOPC, pH 7.0.

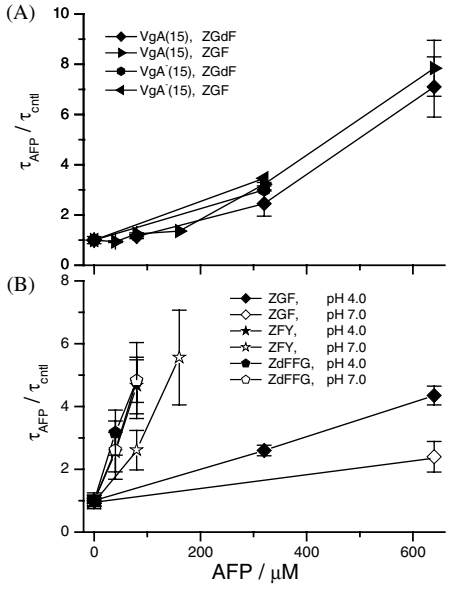

Figure 9. ZGF, ZGdF, ZFT and ZdFFG increase the lifetimes of VgA(15) and VgA$^-$(15) channels. The upper panel shows the changes in the lifetimes of VgA and VgA$^-$(15) channels induced by ZGF and ZGdF in DPhPC bilayers using unbuffered 1.0 M NaCl solutions. As in figure 6, the results are shown as normalized changes in lifetimes ($\tau_{\mathrm{AFP}}/\tau_{\mathrm{cntl}}$); $\tau_{\mathrm{cntl}} \approx 600$ ms. The lower panel shows the changes in the lifetime of VgA channels induced by ZGF, ZFT and ZdFFG in DPhPC bilayers in 1.0 M NaCl solution buffered to pH 4.0 (solid symbols) and pH 7.0 (open symbols). The control lifetimes were similar at pH 4.0 and pH 7.0.

3.2. pH dependence of the anti-fusion peptide modulation of gramicidin channel function

The initial experiments in this study were done with VgA(15) and VgA$^-$(15) and ZGF and ZGdF in unbuffered 1.0 M NaCl solutions in DPhPC/ *n*-decane bilayers (figure 9(A)).

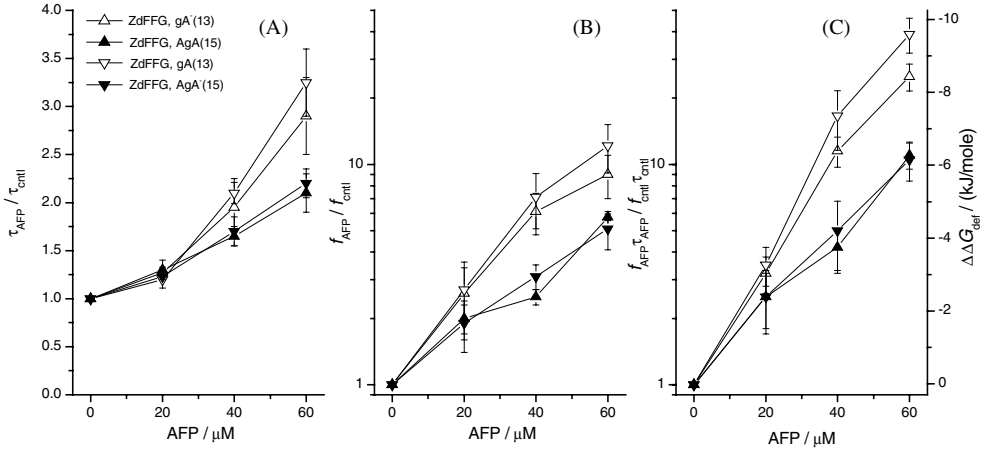

Figure 10. ZdFFG-induced changes in the lifetimes (left panel), appearance rates (middle panel) and time-averaged concentrations and free energy of formation (right panel) of enantiomeric pairs of 13-residue and 15-residue gramicidin channels. In the right panel the left-hand ordinate denotes the relative channel concentrations, expressed as $f_{\rm AFP}\tau_{\rm AFP}/f_{\rm cntl}\tau_{\rm cntl}$, and the right-hand ordinate denotes the changes in the free energy of gramicidin channel formation (cf equation (11)). As in figures 6–8, the open symbols denote results with the 13-residue channels and the filled symbols denote results with the 15-residue channels; the different symbol shapes denote the different experimental conditions: gA$^-$(13) + AgA(15) or gA(13) +AgA$^-$(15). In the absence of ZdFFG, the lifetimes for gA$^-$(13), AgA(15), gA(13) and AgA$^-$(15) channels were 10.2 ± 1.2, 132 ± 7, 13.1 ± 1.4 and 155 ± 9 ms, respectively. DOPC, pH 7.0.

The average lifetimes of the VgA channels are about four times longer than the lifetimes of AgA(15) channels [35] but, consistent with the results obtained with AgA$^-$(15) and AgA(15), the effects of ZGF and ZGdF on the VgA(15) and VgA$^-$(15) channels are similar among the four combinations—again indicating the AFPs act by changing global bilayer properties, as opposed to more specific AFP–channel interactions. As was the case with the AgA$^-$(15) and AgA(15) channels, the AFPs did not alter the magnitudes of the single-channel current transitions (results not shown). The major difference between the results in figures 6 and 9 is the non-linear dose–response curves in the experiments with the unbuffered solutions (figure 9); when we measured the pH changes due to the addition of AFPs, the pH of the solutions turned out to be ∼4 at 120 μM ZGF (or ZGdF), as compared to ∼6 in the absence of the AFPs.

We therefore determined how ZGF, ZFY and ZdFFG altered gA channel lifetimes at pH 4.0 and pH 7.0 (figure 9(B)); the latter compound was chosen to determine whether the rank order of viral anti-fusion activity [71] is similar to the compounds' effect on channel lifetimes. At pH 7.0 the rank-order potency in figure 10 is ZdFFG > ZFY > ZGF, with ZdFFG being about ten times more active than ZGF—similar to that observed for the peptides' anti-viral activity [72]. At pH 4.0, ZFY and ZGF were two to three times more active than at pH 7.0; there was no significant change in the activity of ZdFFG. Again, we did not observe any changes in the single-channel currents. In the case of ZFY, for example, the current magnitudes varied between 3.16 ± 0.09 pA at 0 μM and 3.24 ± 0.08 at 80 μM.

3.3. The changes in gramicidin channel function result from changes in global bilayer properties

The results in figures 6–8 show that the AFP-induced changes in gA channel function do not depend on the chirality of the AFPs or the channels. The results therefore suggest that the

changes in gA channel function are due to AFP-induced changes in global bilayer properties. To provide further support for this suggestion, we examined how ZdFFG, the most potent of the AFPs tested, alters the function of $gA^-(13)$, gA(13), $AgA^-(15)$ and AgA(15) channels (figure 10).

As was the case for the experiments with ZGF and ZGdF, addition of ZdFFG increases the average lifetimes (figure 10(A)) and channel appearance rates (figure 10(B)) of both left- and right-handed channels, again with little effect on the single-channel current transition amplitudes: 2.05 ± 0.13 pA and 3.27 ± 0.12 pA for $gA^-(13)$ and AgA(15) channels in the absence of ZdFFG, as compared to 2.12 ± 0.11 pA and 3.38 ± 0.10, respectively, at 60 μM ZdFFG; comparable results were obtained with gA(13) and $AgA^-(15)$ channels. As would be expected from the results in figure 9, ZdFFG is 20-fold more potent than ZGF or ZGdF (cf figures 6 and 7) in terms of altering τ. ZdFFG also is more potent as an inhibitor of measles virus plaque formation, but the difference in potency is ~2000-fold [72].

The relative changes in τ and f (figures 10(A) and (B)), or in $\Delta G^0_{\rm def}$ (figure 10(C)) do not depend on the channel helix sense. Though we did experiments only with ZdFFG, the similar changes in τ and f observed with $gA^-(13)$ and gA(13) channels, and with $AgA^-(15)$ and AgA(15) channels—taken together with the results obtained with ZGF and ZGdF—allow us to rule out 'specific' channel–AFP interactions. We conclude that the AFP-induced changes in gA channel function result from changes in global bilayer properties.

In contrast to the results with ZGF or ZGdF, the ZdFFG-induced changes in τ and f (and thus $\Delta G^0_{\rm def}$) were larger for the 13-residue channels than for the 15-residue channels (figure 10). That is, the ZdFFG-induced changes in gA channel function depend on the extent of hydrophobic mismatch, which implies that ZdFFG alters not only the monolayer intrinsic curvature but also the bilayer elastic moduli ($H_{\rm B}$ and $H_{\rm X}$ in equation (7)).

3.4. pH dependence of the effect of ZGF and ZGdF

To understand better the basis for the greater effect of ZGF and ZGdF under acidic conditions (cf figure 9(A)), we did experiments at pH 4.0 (figure 11). At pH 4.0, the channel-forming ability (the amount of gA added to the aqueous phases in order to observe comparable appearance rates) was similar to that at pH 7.0 (results not shown). Furthermore, the single-channel lifetimes (see legends to figures 6 and 11) and current transition amplitudes did not vary significantly between pH 7.0 and 4.0: for the 13-residue channels and 15-residue channels, the single-channel current transition amplitudes were 2.11 ± 0.09 pA and 3.33 ± 0.11, respectively, which compares well with the results at pH 7.0 (figure 5(A)). The addition of 400 μM ZGdF did not cause any changes, as the comparable values were 2.04 ± 0.11 pA and 3.32 ± 0.12 pA, respectively.

As would be expected from the results in figure 9, the changes in f and τ (figures 11(A) and (B)) were greater than at pH 7.0. It was not, in fact, possible to make the measurements using [AFP]s $>$ 400 μM because the channel appearance rates became too high. Even at 400 μM, the appearance rate measurements are uncertain, and we do not attach significance to the apparently greater effect of ZGF, as compared to ZGdF. As was the case at pH 7.0, the changes in channel function do not depend on the chirality of the AFP—again consistent with AFP-induced changes in bilayer physical properties. In contrast to the results at pH 7.0, however, at pH 4.0 ZGF and ZGdF cause much greater changes in f and τ (and thus $\Delta G^0_{\rm def}$, figure 11(C)) of the 13-residue channels than of the 15-residue channels. Within the conceptual framework provided by the theory of elastic bilayer deformations, the larger effect on the shorter channels (the dependence on the hydrophobic mismatch) shows that ZGF and ZGdF at pH 4.0 reduce the bilayer elastic moduli (as reflected in the coefficients $H_{\rm B}$ and $H_{\rm X}$).

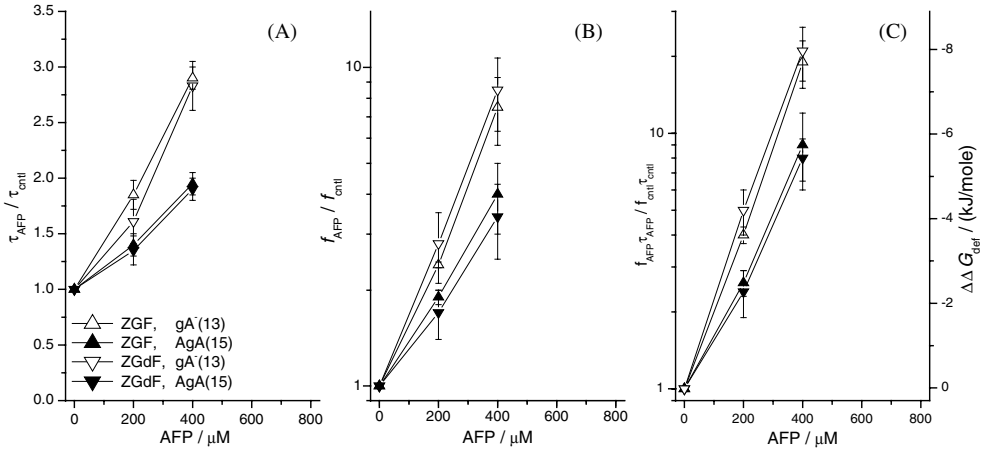

Figure 11. ZGF- and ZGdF-induced changes in the lifetimes (left panel), appearance rates (middle panel) and the time-averaged concentrations and free energy of formation (right panel) of enantiomeric pairs of 13-residue and 15-residue gramicidin channels. In the right panel the left-hand ordinate denotes the relative channel concentrations, expressed as $f_{\rm AFP}\tau_{\rm AFP}/f_{\rm cntl}\tau_{\rm cntl}$, and the right-hand ordinate denotes the changes in the free energy of gramicidin channel formation (cf equation (11)). To facilitate comparison with figures 6–8, we use the same scale for abscissa as on those figures. As in figures 6–8, the open symbols denote results with the 13-residue channels and the filled symbols denote results with 15-residue channels; the different symbol shapes denote the different experimental conditions, $gA^-(13) + AgA(15)$ and either ZGF or ZGdF. DOPC, pH 4.0.

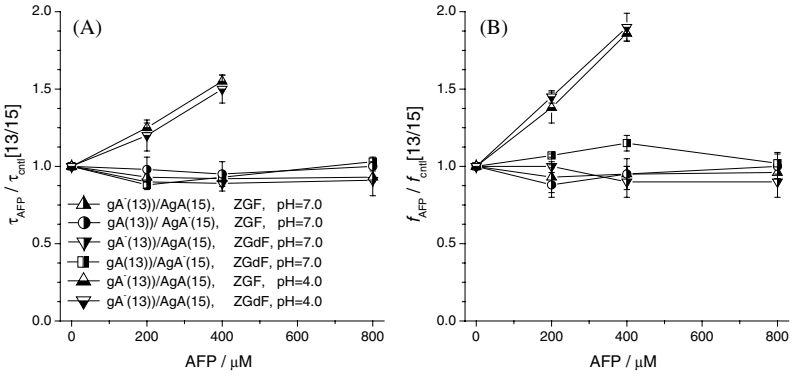

Figure 12. Relative effects of ZGdF and ZGF on gA(13) and $AgA^-(15)$ and on $gA^-(13)$ and AgA(15) channels. The left-hand panel shows the AFP-induced changes in the lifetimes of the 13-residue channels relative to the changes in the lifetimes of the 15-residue channels. The right-hand panel shows the corresponding AFP-induced changes in the appearance rates of the 13-residue channels relative to the changes in the appearance rates of the 15-residue channels. In either panel, a value of 1.0 means that the AFPs have the same effect on the 13-residue and 15-residue channels. DOPC, pH 4.0 and 7.0.

The similarities and differences in the AFP-induced changes in gA channel function at pH 4.0 and 7.0 are illustrated further in figure 12, which compares how the AFPs alter the τs and fs of channels formed by 13-residue and 15-residue subunits: $\tau_{\rm AFP}/\tau_{\rm cntl}$ [13/15] and $f_{\rm AFP}/f_{\rm cntl}$ [13/15], respectively.

At both pHs, the AFP-induced changes in τ (figure 12(A)) and f (figure 12(B)) do *not* depend on the AFP or the channel chirality. (As noted above, we believe that the larger

apparent effect of ZGF on f_{AFP}/f_{cntl} [13/15] is due to uncertainties in the determination of the appearance rates.) At pH 7.0, the AFP-induced changes in τ_{AFP}/τ_{cntl} [13/15] and f_{AFP}/f_{cntl} [13/15] are close to one, meaning that the changes in neither f nor τ depend on the hydrophobic mismatch. At pH 4.0, AFPs have a more pronounced effect on the $gA^-(13)$ channels than on the AgA(15) channels, with comparable changes in τ and f.

The different patterns of the changes in τ_{AFP}/τ_{cntl} [13/15] and f_{AFP}/f_{cntl} [13/15] at pH 7.0 and 4.0 do not result from changes in channel function in the absence of AFP, as neither the lifetimes nor the channel-forming abilities vary between pH 7.0 and 4.0. We conclude that the bilayer physical properties do not vary between pH 7.0 and 4.0, meaning that the differences must arise from differences in the AFP–bilayer interactions. As the pK of the free carboxyl group of small oligopeptides is ∼3.5 [17], the concentration of the protonated AFP will be three orders of magnitude higher at pH 4.0 than at pH 7.0. The dose–response curves for the changes in τ at pH 7.0 and 4.0 (figures 6 and 11(A)), however, show that the AFPs are about twice as potent at pH 4.0 as at 7.0. Based on the lifetime changes we therefore conclude that adsorption of both the charged and uncharged (protonated) AFPs alters bilayer physical properties, but that the uncharged form is more effective. Within the framework provided by equations (7)–(9) the charged AFPs have their predominant effect on the lipid intrinsic curvature, whereas the uncharged AFPs also alter bilayer elasticity. In contrast to the predictions of the theory of elastic bilayer deformations, however, the AFP-induced changes in channel appearance rates are similar for the 13-residue and 15-residue channels, meaning that we do not observe the expected dependence on the channel–bilayer hydrophobic mismatch.

4. Discussion

We show how small hydrophobic/amphipathic peptides can alter bilayer physical properties, using gA channels as probes of bilayer properties. The AFP-induced changes in channel properties do not depend on the chirality of either the channel-forming molecules or the AFPs. One can thus exclude that the changes in gA channel function result from specific AFP–channel interactions. Rather, the AFPs alter gA channel function by altering global bilayer properties. The gA channels therefore are suitable as probes to monitor how small amphiphiles alter global bilayer properties, a conclusion that confirms and extends our previous work [4, 35, 50, 52–54].

The adsorption of small amphiphiles at the bilayer/solution interface may alter one or more different bilayer properties, e.g. fluidity [24, 33], lipid intrinsic curvature [79, 84], thickness [92], and bilayer elastic moduli [18, 55, 75, 92]. These changes in bilayer properties are not mutually exclusive, which complicates attempts to understand the bilayer regulation of membrane protein function. Though changes in membrane fluidity have been invoked (see, e.g., Aloia *et al* [2]), there is considerable evidence that changes in bilayer fluidity *per se* cannot be a major regulator of membrane protein function [28, 46]. Most importantly, changes in fluidity cannot be invoked to account for changes in the equilibrium distribution among different membrane protein conformations, including the gA monomer ↔ dimer equilibrium.

By contrast, changes in lipid intrinsic curvature and bilayer elastic moduli, which will alter the energetics of protein-induced bilayer perturbations, would be able to alter the equilibrium distribution between different protein conformations. Long ago it was pointed out that progress in understanding how the host lipid bilayer regulates the function of the imbedded proteins will depend on examining the energetics of how changes in bilayer properties alter membrane protein function [27]. Generally, however, the adsorption of an amphiphile that alters the bilayer elastic moduli will be expected to alter also lipid intrinsic curvature, and *vice versa*, because both the elastic moduli and the curvature are determined by the profile of lateral intermolecular interactions through the bilayer [32, 79]. Changes in either elastic moduli or

intrinsic curvature may dominate, and it becomes important to determine which contribution is the most important and relevant for understanding changes in membrane protein function.

Because the formation of gA channels causes a local bilayer thinning, as the channels form by the transbilayer dimerization of two non-conducting subunits (figure 2), gA channels have the potential to provide information about how bilayer-spanning proteins sense changes in bilayer physical properties. Though the conformational changes in integral membrane proteins differ from the gA monomer ↔ dimer equilibrium, cf figures 1 and 2, gA channels are *in situ* force transducers that provide information about how changes in bilayer properties may alter the energetics of changes in protein–bilayer hydrophobic mismatch [4]. It is in this context important that the atomic resolution structure of the bilayer-spanning gA channels is known [43] and robust with respect to the effects of amino acid substitutions [1, 39, 80, 85], and that the mechanism of channel formation is known, being a transbilayer dimerization of two non-conducting monomers [64]. Taken together with the perpendicular orientation of the bilayer-spanning channels [12, 44, 61], it thus becomes possible to relate changes in single-channel lifetimes to changes in the disjoining force the bilayer imposes on the channel—and to relate changes in integral membrane protein function to changes in gA channel lifetimes [52, 53].

There is no atomic resolution structure for the non-conducting dimers, which may complicate the interpretation of the channel appearance rates. Three observations, however, provide support for the notion that the channels form by the dimerization of $\beta^{6.3}$-helical monomers residing in each bilayer leaflet: first, the conducting channels form by the transbilayer dimerization of non-conducting monomers, without a need to unfold from another conformation [64]. Second, non-conducting $\beta^{6.3}$-helical monomers can be imbedded into each bilayer leaflet [29]. Third, even in aqueous solutions, gA folds into surprisingly tight monomers at low (picomolar) concentrations [38]. A comparison of the energetic penalty associated with having six potentially hydrogen-bonding residues buried in the bilayer interior ($\sim$20 kcal mol^{-1}, cf Fersht [20]), with the hydrophobic penalty of having a folded $\beta^{6.3}$-helical monomer at the bilayer/solution interface, with its axis parallel to the bilayer ($\sim$25 kcal mol^{-1} using a hydrophobic penalty of $\sim$50 cal Å^{-2}, cf Dill *et al* [14]), likewise supports the notion of transbilayer dimerization of bilayer-imbedded $\beta^{6.3}$-helical monomers.

Though we cannot exclude that the AFPs cause small changes in bilayer thickness, the observation that the relative AFP-induced changes in channel lifetimes at pH 7.0 do not depend on the channel-bilayer hydrophobic mismatch (figures 6 and 12(A)) suggests that ZGF and ZGdF alter bilayer properties by changing lipid intrinsic curvature without changing the bilayer elastic moduli (actually the coefficient H_B, which is a function of the bilayer area-compression and bending moduli). At pH 4.0, ZGF and ZGdF do produce changes in H_B. The difference between the AFP effects at pH 7.0 and pH 4.0 is likely due to a deeper penetration into the bilayer of the neutral (uncharged) forms of ZGF and ZGdF. Surprisingly, however, we did not observe the expected channel length-dependent changes in the appearance rates for the 13-residue and 15-residue channels that would be predicted from the expression for $\Delta G^0_{\rm def}$; cf equation (5). We do not understand why not. Though the continuum theory of elastic bilayer deformations appears to provide a robust tool for understanding how membrane protein function can be regulated by the host bilayer, the neglect of molecular detail may be problematic.

ZdFFG is more potent than ZGF as an inhibitor of viral fusion and as a modifier of bilayer properties, though the 100-fold difference in the relative potencies of ZdFFG and ZGF as fusion inhibitors and as bilayer modifiers suggests that the anti-fusion activity (for ZdFFG, at least) is not the direct consequence of changes in bilayer properties. This suggestion needs to be tempered, however, because viral fusion is likely to involve a larger membrane area than would

be perturbed by a single gA channel. In any case, ZdFFG causes similar changes in the function of left-and right-handed channels, which provides additional support for the notion that viral anti-fusion peptides can alter global bilayer properties—and that the changes in gA channel function result from these changes in global bilayer properties, and not from more direct AFP–channel interactions. The observation that ZdFFG has a larger effect on the shorter 13-residue channels than the longer 15-residue channels could suggest that the more hydrophobic ZdFFG can penetrate deeper into the bilayer core than ZGF, consistent with the different effects of ZGF itself at pH 7.0 and 4.0. By analogy to other charged peptides [91], the charges are likely to preferentially reside in the outer part of the phospholipid head group region, with the rest of the molecule in closer contact with the bilayer hydrophobic core.

Finally we note that just as the channel–bilayer interaction causes a bilayer deformation one would also expect to have changes in the channel structure—even if proteins are less compressible than the bilayer lipids [23, 49]. Consistent with previous structural studies [41, 88], any such changes in gA channel structure are likely to be small because we observe no changes in the single-channel conductance, which would be expected to vary with changes in the peptide backbone structure. That is, one can to a first approximation regard the channels as being rigid entities imbedded in a soft membrane.

5. Conclusion

Anti-fusion peptides alter gA channel function by mechanisms that do not depend on the chirality of the channel-forming gAs or the AFPs. We thus can exclude that specific channel–AFP interactions are involved, and conclude that the AFPs alter global bilayer physical properties by causing a more positive monolayer intrinsic curvature (at pH 7 where the anti-fusion peptides bear a negative charge), or by changing both bilayer elasticity and monolayer curvature (at pH 4 where the anti-fusion peptides are more neutral). The AFPs do not cause measurable changes in the single-channel currents through the bilayer-spanning channels themselves, indicating that the changes in the disjoining force the bilayer imposes on the channel have little, if any, impact on the channel structure. Our results thus confirm and extend previous results, that gA channels constitute a powerful tool to monitor changes in bilayer physical properties—in a manner that is relevant for understanding how changes in lipid bilayer properties regulate integral membrane protein function.

Acknowledgments

This work was supported in part by NIH grants GM21342 (OSA) and RR15569 (DVG and REK). We thank Michel J Bruno, Helgi Ingolfsson, Jens A Lundbæk, Jon Sack and Shobana Sundaram for stimulating discussions.

References

[1] Allen T W, Andersen O S and Roux B 2003 *J. Am. Chem. Soc.* **125** 9868–78
[2] Aloia R C, Curtain C C and Gordon L M 1988 *Advances in Membrane Fluidity* vol 1 *Methods for Studying Membrane Fluidity*
[3] Andersen O S 1983 *Biophys. J.* **41** 119–33
[4] Andersen O S, Nielsen C, Maer A M, Lundbæk J A, Goulian M and Koeppe R E II 1999 *Meth. Enzymol.* **294** 208–24
[5] Andersen O S, Sawyer D B and Koeppe R E II 1992 *Biomembrane Structure and Function* ed K R K Easwaran and B Gaber (Schenectady, NY: Adenine Press) pp 227–44
[6] Arseniev A S, Barsukov I L, Bystrov V F and Ovchinnikov Yu A 1986 *Biol. Membr.* **3** 437–62

[7] Bamberg E and Läuger P 1973 *J. Membr. Biol.* **11** 177–94
[8] Benz R, Fröhlich O, Läuger P and Montal M 1975 *Biochim. Biophys. Acta* **394** 323–34
[9] Borisenko V *et al* 2003 *Biophys. J.* **84** 612–22
[10] Brown M F 1994 *Chem. Phys. Lipids* **73** 159–80
[11] Colquhoun D 1973 *Drug Receptors* ed H P Rang (London: MacMillan Press) pp 149–82
[12] Cornell B A, Separovic F, Baldassi A J and Smith R 1988 *Biophys. J.* **53** 67–76
[13] Dan N and Safran S A 1998 *Biophys. J.* **75** 1410–4
[14] Dill K A, Truskett T M, Vlachy V and Hribar-Lee B 2005 *Annu. Rev. Biophys. Biomol. Struct.* **34** 173–99
[15] Durkin J T, Koeppe R E II and Andersen O S 1990 *J. Mol. Biol.* **211** 221–34
[16] Durkin J T, Providence L L, Koeppe R E II and Andersen O S 1993 *J. Mol. Biol.* **231** 1102–21
[17] Edsall J T and Wyman J 1958 *Biophys. Chem.* **1**
[18] Evans E, Rawicz W and Hofmann A F 1995 *Bile Acids in Gastroenterology Basic and Clinical Advances* ed A F Hofmann, G Paumgartner and A Stiehl (Dordrecht: Kluwer–Academic) pp 59–68
[19] Evans E A and Hochmuth R M 1978 *Curr. Top. Membr. Transp.* **10** 1–64
[20] Fersht A R 1987 *TIBS* **12** 301–4
[21] Finkelstein A 1976 *J. Gen. Physiol.* **68** 127–35
[22] Finkelstein A 1987 *Water Movement Through Lipid Bilayers, Pores, and Plasma Membranes. Theory and Reality.*
[23] Gekko K and Hasegawa Y 1986 *Biochemistry* **25** 6563–71
[24] Goñi F M, Urbaneja M A, Arrondo J L, Alonso A, Durrani A A and Chapman D 1986 *Eur. J. Biochem.* **160** 659–65
[25] Greathouse D V, Koeppe R E II, Providence L L, Shobana S and Andersen O S 1999 *Meth. Enzymol.* **294** 525–50
[26] Gruner S M 1985 *Proc. Natl Acad. Sci. USA* **82** 3665–9
[27] Gruner S M 1991 *Biologically Inspired Physics* ed L Peliti (New York: Plenum) pp 127–35
[28] Hazel J R 1995 *Annu. Rev. Physiol.* **57** 19–42
[29] He K, Ludtke S J, Wu Y, Huang H W, Andersen O S, Greathouse D and Koeppe R E II 1994 *Biophys. Chem.* **49** 83–9
[30] Helfrich P and Jakobsson E 1990 *Biophys. J.* **57** 1075–84
[31] Helfrich W 1973 *Z. Naturf.* c **28** 693–703
[32] Helfrich W 1981 *Physique des Défauts (Physics of Defects)* ed R Balian, M Kléman and J-P Poirier (New York: North-Holland) pp 716–55
[33] Hoekstra F A and Golovina E A 2002 *Comp. Biochem. Physiol.* A **131** 527–33
[34] Huang H W 1986 *Biophys. J.* **50** 1061–70
[35] Hwang T C, Koeppe R E II and Andersen O S 2003 *Biochemistry* **42** 13646–58
[36] Israelachvili J N 1977 *Biochim. Biophys. Acta* **469** 221–5
[37] Jackson M B 1989 *Proc. Natl Acad. Sci. USA* **86** 2199–203
[38] Jagannadham M V and Nagaraj R 2005 *Biopolymers* **80** 708–13
[39] Jordan J B, Easton P L and Hinton J F 2005 *Biophys. J.* **88** 224–34
[40] Karlin A 1967 *J. Theor. Biol.* **16** 306–20
[41] Katsaras J, Prosser R S, Stinson R H and Davis J H 1992 *Biophys. J.* **61** 827–30
[42] Kelsey D R, Flanagan T D, Young J E and Yeagle P L 1991 *Virology* **182** 690–702
[43] Ketchem R R, Roux B and Cross T A 1997 *Structure* **5** 1655–69
[44] Killian J A, Taylor M J and Koeppe R E II 1992 *Biochemistry* **31** 11283–90
[45] Koeppe R E II, Providence L L, Greathouse D V, Heitz F, Trudelle Y, Purdie N and Andersen O S 1992 *Proteins* **12** 49–62
[46] Lee A G 1991 *Prog. Lipid Res.* **30** 323–48
[47] Lee A G 2004 *Biochim. Biophys. Acta* **1666** 62–87
[48] Lewis B A and Engelman D M 1983 *J. Mol. Biol.* **166** 211–7
[49] Liu N and Kay R L 1977 *Biochemistry* **16** 3484–6
[50] Lundbæk J A and Andersen O S 1994 *J. Gen. Physiol.* **104** 645–73
[51] Lundbæk J A and Andersen O S 1999 *Biophys. J.* **76** 889–95
[52] Lundbæk J A, Birn P, Tape S E, Toombes G E, Sogaard R, Koeppe R E II, Gruner S M, Hansen A J and Andersen O S 2005 *Mol. Pharmacol.* **68** 680–9
[53] Lundbæk J A, Birn P H A J, Søgaard R, Nielsen C, Girshman J, Bruno M J, Tape S E, Egebjerg J, Greathouse D V, Mattice G L, Koeppe R E II and Andersen O S 2004 *J. Gen. Physiol.* **123** 599–621
[54] J A Lundbæk, Maer A M and Andersen O S 1997 *Biochemistry* **36** 5695–701
[55] Ly H V and Longo M L 2004 *Biophys. J.* **87** 1013–33
[56] McLaughlin S 1977 *Curr. Top. Membr. Transp.* **9** 71–144
[57] Miloshevsky G V and Jordan P C 2004 *Biophys. J.* **86** 92–104

[58] Mouritsen O G and Andersen O S (ed) 1998 *In Search of a New Biomembrane Model. Biol. Skr. Dan. Vid. (Munksgaard, Copenhagen: B)*
[59] Mouritsen O G and Bloom M 1984 *Biophys. J.* **46** 141–53
[60] Muller R U and Finkelstein A 1972 *J. Gen. Physiol.* **60** 285–306
[61] Nicholson L K, Moll F, Mixon T E, LoGrasso P V, Lay J C and Cross T A 1987 *Biochemistry* **26** 6621–6
[62] Nielsen C, Goulian M and Andersen O S 1998 *Biophys. J.* **74** 1966–83
[63] Nielsen C and Andersen O S 2000 *Biophys. J.* **79** 2583–604
[64] O'Connell A M, Koeppe R E II and Andersen O S 1990 *Science* **250** 1256–9
[65] Orbach E and Finkelstein A 1980 *J. Gen. Physiol.* **75** 427–36
[66] Partenskii M B and Jordan P C 2002 *J. Chem. Phys.* **117** 10768–76
[67] Perozo E, Cortes D M and Cuello L G 1999 *Science* **285** 73–8
[68] Perozo E, Cortes D M, Sompornpisut P, Kloda A and Martinac B 2002 *Nature* **418** 942–8
[69] Providence L L, Andersen O S, Greathouse D V, Koeppe R E II and Bittman R 1995 *Biochemistry* **34** 16404–11
[70] Razinkov V I, Melikyan G B, Epand R M, Epand R F and Cohen F S 1998 *J. Gen. Physiol.* **112** 409–22
[71] Richardson C D and Choppin P W 1983 *Virology* **131** 518–32
[72] Richardson C D, Scheid A and Choppin P W 1980 *Virology* **105** 205–22
[73] Ring A 1996 *Biochim. Biophys. Acta* **1278** 147–59
[74] Sackmann E 1984 *Biological Membranes* ed D Chapman (London: Academic) pp 105–43
[75] Santore M M, Discher D E, Won Y-Y, Bates F S and Hammer D A 2002 *Langmuir* **18** 7299–308
[76] Sawyer D B and Andersen O S 1989 *Biochim. Biophys. Acta* **987** 129–32
[77] Sawyer D B, Koeppe R E II and Andersen O S 1989 *Biochemistry* **28** 6571–83
[78] Schatzberg P 1965 *J. Polym. Sci.* C **10** 87–92
[79] Seddon J M 1990 *Biochim. Biophys. Acta* **1031** 1–69
[80] Sham S S, Shobana S, Townsley L E, Jordan J B, Fernandez J Q, Andersen O S, Greathouse D V and Hinton J F 2003 *Biochemistry* **42** 1401–9
[81] Simon S A, McIntosh T J and Latorre R 1982 *Science* **216** 65–7
[82] Singer S J and Nicolson G L 1972 *Science* **175** 720–31
[83] Szabo G, Eisenman G and Ciani S 1969 *J. Membr. Biol.* **1** 346–82
[84] Tate M W, Eikenberry E F, Turner D C, Shyamsunder E and Gruner S M 1991 *Chem. Phys. Lipids* **57** 147–64
[85] Townsley L E, Tucker W A, Sham S and Hinton J F 2001 *Biochemistry* **40** 11676–86
[86] Toyoshima C and Mizutani T 2004 *Nature* **430** 529–35
[87] Unwin P N T and Ennis P D 1984 *Nature* **307** 609–13
[88] Wallace B A, Veatch W R and Blout E R 1981 *Biochemistry* **20** 5754–60
[89] Walter A and Gutknecht J 1986 *J. Membr. Biol.* **77** 255–64
[90] Yeagle P L, Young J, Hui S W and Epand R M 1992 *Biochemistry* **31** 3177–83
[91] Zhang W, Crocker E, McLaughlin S and Smith S O 2003 *J. Biol. Chem.* **278** 21459–66
[92] Zhou Y and Raphael R M 2005 *Biophys. J.* **89** 1789–801